INTERNATIONAL JOURNAL FOR NUMERICAL METHODS IN FLUIDS
Int. J. Numer. Meth. Fluids 2003; **43**:281–299 (DOI: 10.1002/fld.610)

A block-implicit numerical procedure for simulation of buoyant swirling flows in a model furnace

Marcelo J. S. de Lemos*,†

Departamento de Energia-IEME, Instituto Tecnológico de Aeronáutica-ITA, 12228-900 São José dos Campos, S.P., Brazil

SUMMARY

This work reports numerical results for the case of incompressible laminar heated flow with a swirl in a vertical cylindrical chamber. Computations are obtained with a point-wise block-implicit scheme. Flow governing equations are written in terms of the so-called primitive variables and are recast into a general form. The discretized momentum equations are applied to each cell face and then, together with the mass-continuity, tangential velocity and energy equations, are solved directly in each computational node. The effects of Rayleigh, Reynolds and Swirl numbers on the temperature field are discussed. Flow pattern and scalar residual history are reported. Further, it is expected that more advanced parallel computer architectures can benefit from the error smoothing operator here described. Copyright © 2003 John Wiley & Sons, Ltd.

KEY WORDS: model furnace; numerical methods; implicit solution; coupled solution; buoyancy

INTRODUCTION

The growing trend in environment regulations points towards ever tighter pollutant release limits of modern combustion systems. Today, new technologies for efficient energy production are based on the so-called lean and low-NO_x combustion. Accordingly, most flow fields in such systems are characterized by an ascending stream with an induced swirling motion. Swirling induces flame stabilization allowing peak temperature reduction, ultimately reducing pollutant formation rates. Recently, the design and analysis of such systems, driven by increased microprocessor performance and associated low computational costs, have made systematic use of numerical tools. In the end, the growing number of available software packages for fluid system design has helped engineers in reducing the necessary time before a new concept is finally available in the market.

In spite of the increasing use of CFD tools, the numerical solution of such flows imposes additional difficulties due to the intricate coupling between *temperature*, *tangential*

*Correspondence to: M. J. S. de Lemos, Departamento de Energia-IEME, Instituto Tecnólogico de Aeronáutica-ITA, 12228-900 São José dos Campos, S.P., Brazil.
†E-mail: delemos@mec.ita.br

Received January 2000
Revised 30 January 2003

velocity and *cross-flow* fields. Buoyancy term, centripetal and Coriollis accelerations make the system of governing equations of a high degree of coupling. For instance, for a system oriented vertically, with the W-component of velocity in the vertical direction, the temperature T appears in the W-equation. Also, the radial U-component of velocity is governed by an equation that includes the V-component in the centripetal acceleration term. In addition, the tangential velocity V is affected by U through the Corriolis acceleration. Therefore, U,W,V and T are further connected to each other when buoyancy and rotation are simultaneously present in the flow, increasing the aforementioned degree of coupling among all variables involved.

Linearization of governing equations followed by the use of iterative solvers is the common route found in the literature for solving such nonlinear problems. Accordingly, the rate of convergence of any algorithm is essentially dictated by the degree in which physical coupling is mimicked by the method in question. Ultimately, this is an indication that numerical solutions of swirling flows, in most cases, suffer from the disadvantage of longer computing times when compared to their non-swirling counterpart.

Segregated methods, in which one individual flow variable is relaxed while holding the others still, are known to be rather sensitive when handling strong physical coupling. For that, the so-called *coupled* solvers, where all dependent variables are relaxed in the same domain location, have received much attention lately.

For buoyancy-driven laminar flows, bench mark solutions for the field in a square cavity have been presented [1]. Multi-grid solution for this problem has also been published [2]. In the great majority of those works, a segregated method is generally employed with the repetitive solution of a pressure or pressure-correction equation, followed by subsequent updates of the velocity and scalar fields. This strategy forms the basis of the SIMPLE family of algorithms [3]. Coupled line solvers for the temperature and velocity fields have shown improvements in computer time requirements for natural convection flows with large Rayleigh numbers [4]. The work in Reference [4] is an indication of the advantage of coupled schemes for solving algebraic equations set with a high degree of interlinkage among the variables. Recently, the block implicit technique has also been applied in the calculation of buoyant flows in a partially-coupled manner [5].

For swirling flows, most solutions found in the literature are also based on segregated relaxation procedures [6–8]. In the present context, a fully-implicit treatment is associated with the idea of simultaneously updating flow and scalar fields at each step within the error smoothing operator. To the best of the author's knowledge, in all published work, neither temperature nor tangential velocity fields, seen here as *scalars*, are treated in a fully implicit manner.

Following the aforementioned and based on Vanka's SGCS method [9, 10], De Lemos [11] simulated lid-driven cavity fluid motion through a cylindrical tank using a block-implicit numerical scheme. In addition, the same algorithm has been applied to calculation of swirling flows in model combustor [12]. Later, the technique was extended to buoyancy-driven streams [13], including vertical [14] and inclined cavities [15]. Recently, full documentation of coupled treatment for swirling [16] and buoyant flows [17] has been made available in the open literature. In those papers, a fully-implicit treatment for the scalar quantities (temperature or tangential velocity) has been made use.

The objective of this paper is to further extend the technique presented in References [12, 16] for the azimuthal velocity and in References [12–15, 17] for temperature, combining

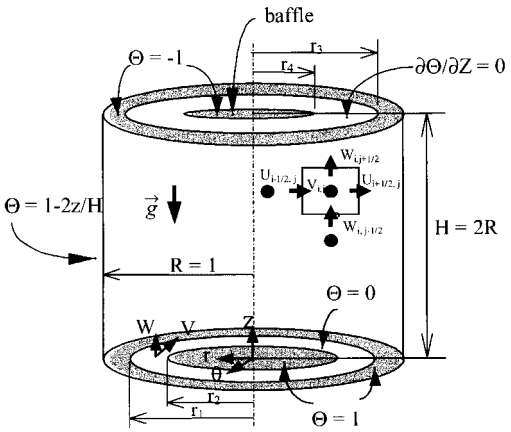

Figure 1. Vertical cylindrical chamber.

now the solution of both scalars into a single fully-implicit numerical treatment. To this end, computations are presented for a model furnace comprising incompressible laminar flow simultaneously heated and subjected to an incoming flow with swirl. Effects of Reynolds, Rayleigh number and swirling strength on temperature patterns and convergence rates are reported.

GOVERNING EQUATIONS AND NUMERICAL METHOD

Geometry

The geometry here considered is schematically shown in Figure 1. A typical furnace combustion zone is approximated by a model consisting of a circular chamber of constant radius R. At inlet, the mixture air+fuel enters through a circular slot of clearance $r_1 - r_2$. At one diameter downstream the entrance, combustion gases are able to exit through an annulus of thickness $r_3 - r_4$. The temperature level is prescribed over the entire lateral wall and on the bottom and top lids, except at the exit area where a null temperature gradient is assumed to be established by the outward motion of the fluid.

Although it is recognized that the geometry of Figure 1 might be an oversimplification of state-of-the-art of industrial furnaces, essential elements, namely *swirl*, *buoyancy* and *recirculating zones* provide a good test case for the numerical method here discussed.

Compact notation

The conservation equations for mass, momentum and energy here analysed can be written in a compact form if the existing analogies among the processes of accumulation, transport, convection and generation/destruction of those quantities are observed. This generic equation is commonly known in the literature as the *general transport equation* and can be written in

Table I. Terms in the general transport.

	ϕ	Γ^ϕ	S^ϕ
Continuity	1	0	0
Axial momentum	W	μ	$-\dfrac{\partial P}{\partial z}+\rho g_z\beta(T-T_0)$
Radial momentum	U	μ	$-\left(\dfrac{\partial P}{\partial r}+\dfrac{\mu U}{r^2}-\dfrac{\rho V^2}{r}\right)$
Azimuthal momentum	V	μ	$-\left(\dfrac{\mu V}{r^2}+\dfrac{\rho UV}{r}\right)$
Energy	T	μ/Pr	0

its *conservative* two-dimensional form for *axi-symmetric* laminar cases as

$$\frac{\partial}{\partial z}\left[\rho W\phi-\Gamma^\phi\frac{\partial\phi}{\partial z}\right]+\frac{1}{r}\frac{\partial}{\partial r}\left[r\left(\rho U\phi-\Gamma^\phi\frac{\partial\phi}{\partial r}\right)\right]=S^\phi \tag{1}$$

In Equation (1) ϕ can represent any quantity of vectorial or scalar nature (velocity or temperature), ρ is the fluid density, U and W are the velocity components in the r- and z-directions, respectively, Γ^ϕ is the transport coefficient for diffusion and S^ϕ is the source term. Table I identifies corresponding terms for the different equations represented by (1). In both Table I and Equation (1) gravity acts in the z-direction, μ is the fluid viscosity, Pr the Prandtl number, T the temperature and V the tangential velocity component.

Boundary conditions

Boundary conditions used for all velocity components were given value at the flow inlet and non-slip condition at chamber walls. For cells facing the outlet plane, overall mass-conservation balance at each computational cell was used to calculate the control-volume outgoing axial velocity (at the top lid). Initial null values were set for all velocities.

For temperature, a linear profile along the vertical direction was assumed to prevail over the lateral wall (see Figure 1). Except in the opened areas, at the bottom and at the top, the non-dimensional temperature took the values $+1$ and -1, respectively. Through the inlet and outlet areas, the applied boundary conditions for the temperature were $\Theta=0$ and $\partial\Theta/\partial z=0$, respectively.

Numerical implementation of boundary conditions was achieved by maintaining the constant initial values at the boundaries, where applicable, or by updating them at each iteration, as in the cases of outlet surfaces or symmetry line.

All computations below used a 18×36 *single* grid equally distributed in the calculation domain. An essential characteristic of Vanka's work, the *multigrid* artifice, has *not* been used in the present work due to the relatively modest grid analysed here. Multigrid techniques are known to perform well with mid-size to large grids [18], but are rather ineffective when applied

to small size problems. For this reason, no multigrid or any other large grid accelerating scheme was implemented.

Computational grid and finite-difference formulation

In this work, the set of equations for mass, momentum and energy above is *differentiated* by means of the widely-used control-volume approach of Patankar, 1980 [3]. The differential equations are integrated over each volume yielding a set of algebraic equations. Internodal variation for the dependent variables can be of different kind corresponding to different *finite-difference* formulations. In the present work, for simplicity, the *Upwind Differencing Scheme* is used to model convective fluxes across volume faces. However, the formulation below is presented in such way that no difficulties arise if another differencing scheme is employed.

Discretized equations

The block-implicit arrangement below for the flow and continuity equations, as mentioned, was first presented by Vanka [9, 10]. For the sake of completeness when extending it to buoyant and swirling problems, the flow equations are here also included. Integrating then the continuity equation around point (ij) (see notation in Figure 1) following standard practices in numerical differentiation, one has [3]

$$F_i^1 U_{i+1/2,j} - F_i^2 U_{i-1/2,j} + F_j^1 W_{i,j+1/2} - F_j^2 W_{i,j-1/2} = 0 \tag{2}$$

where the geometric coefficients Fs make computations convenient and efficient and can be interpreted as (area of flow)/(volume of computational node).

For the radial momentum equation the final form for the $U_{i-1/2,j}$ component contains coefficients representing influences by convection and diffusion mechanisms in addition to all sources and pressure gradient terms. For application in the numerical algorithm below, the equation can be written in such a way that [12]

$$U_{i-1/2,j} = \hat{U}_{i-1/2,j} + \hat{d}_{i-1/2}[P_{i-1,j} - P_{i,j}] + \left(\frac{V_{i,j} + V_{i-1,j}}{2}\right)^2 \frac{1}{a^u_{i-1/2} r_{i-1/2}} \tag{3}$$

where

$$\hat{d}_{i-1/2} = \frac{A_{i-1/2}}{\rho a^u_{i-1/2}} \tag{4}$$

$$\hat{U}_{i-1/2,j} = \frac{\sum_{nb=1}^{4} a^u_{nb} U_{nb} + f^u_{i-1/2}}{a^u_{i-1/2}} \tag{5}$$

and the last term on (3) represents the discrete form on the *centripetal* acceleration shown in Table I. Any other discrete term is accounted for in the "f" parameter. Equation (3) can be further manipulated to give

$$U_{i-1/2,j} = \hat{U}_{i-1/2,j} + \hat{d}_{i-1/2}[P_{i-1,j} - P_{i,j}] + \hat{e}_{i-1/2} V_{i,j} \tag{6}$$

where

$$\hat{e}_{i-1/2} = \frac{(V_{i,j} + V_{i-1,j})}{2r_{i-1/2}a^u_{i-1/2}} \tag{7}$$

and the pseudo-velocity $\hat{U}_{i-1/2,j}$ has been modified for accommodating all remaining terms. Further, in (6) the last term on the right hand side represents the influence of V on the radial velocity U and entails a linearization of the *centripetal* acceleration (see details in References [12, 16]). All sources terms, except the pressure gradient and the contribution due to the tangential velocity, are compacted in the first term on the right-hand side. For the coupled treatment here presented, the explicit contribution of V in the source term of U is necessary, as it will be seen below.

A similar equation for the axial velocity component $W_{i,j-1/2}$ is given by

$$W_{i,j-1/2} = \hat{W}_{i,j-1/2} + \hat{d}_{j-1/2}[P_{i,j-1} - P_{i,j}] + \frac{g_z\beta(T_1 - T_0)}{a^w_{j-1/2}}\left(\frac{\Theta_{i,j} + \Theta_{i,j-1}}{2}\right) \tag{8}$$

where,

$$\hat{d}_{i-1/2} = \frac{A_{j-1/2}}{\rho a^w_{j-1/2}} \tag{9}$$

$$\hat{W}_{j-1/2} = \frac{\sum_{nb=1}^{4} a^w_{nb}U_{nb} + f^w_{j-1/2}}{a^w_{j-1/2}} \tag{10}$$

In (8) β is the thermal expansion coefficient and g_z is the z-component of the gravity vector. For natural convection flows oriented as in Figure 1, the non-dimensional temperature Θ appearing in (11) is defined as $\Theta = (T - T_0)/(T_1 - T_0)$ and is based on the maximum temperature drop across the computational domain $\Delta T = (T_1 - T_0)$. Further rearranging (8), one has

$$W_{i,j-1/2} = \hat{W}_{i,j-1/2} + \hat{d}_{j-1/2}[P_{i,j-1} - P_{i,j}] + \hat{g}_{j-1/2}\Theta_{i,j} \tag{11}$$

where

$$\hat{g}_{j-1/2} = \frac{g_z\beta(T_1 - T_0)}{2a^w_{j-1/2}} \tag{12}$$

Here also the pseudo-velocity $\hat{W}_{i,j-1/2}$ has been modified for including all additional terms (details in Reference [17]). Similarly to what has been mentioned above, it is important to notice that the source term in (11) explicitly shows the contribution of T (or Θ) on W. For the coupled treatment here presented, this explicit arrangement is also as shown later.

Following a similar procedure for the Θ and V equations, final finite-difference equations can be assembled in the following form:

$$a^\Theta_{ij}\Theta_{i,j} = b^\Theta_{ij}\Theta_{i+1,j} + c^\Theta_{ij}\Theta_{i-1,j} + d^\Theta_{ij}\Theta_{i,j+1} + e^\Theta_{ij}\Theta_{i,j-1} \tag{13}$$

$$a^v_{ij}V_{i,j} = b^v_{ij}V_{i+1,j} + c^v_{ij}V_{i-1,j} + d^v_{ij}V_{i,j+1} + e^v_{ij}V_{i,j-1} + f^v_{ij} + g^v_{ij}U_{i,j} \tag{14}$$

It is interesting to observe that the last term in (14) comes from discretization of the *Coriollis* acceleration in the V-equation and represents the feedback effect of the cross-flow on the tangential velocity (see Table I). Consideration of the Corriollis acceleration in the block-implicit treatment shown below would hamper a proper matrix arrangement suitable for fast inversion. This point will be clear after presenting the Numerical Strategy in the next section. In this work, however, this term is not treated implicitly and, when solving for V, it is compacted in the explicitly-treated source term. The *centripetal* acceleration, however (see Table I and Equation (6)), is here implicitly handled. The explicit treatment is also employed when discretizing the *convection* terms in the T and V equations since no particular terms with Us or Ws are shown in (13)–(14).

For simplicity, Equations (13)–(14) can be rearranged such that

$$\Theta_{i,j} = \hat{\Theta}_{i,j}; \quad V_{i,j} = \hat{V}_{i,j} \tag{15}$$

where,

$$\begin{aligned} \hat{\Theta}_{i,j} &= \{b^{\Theta}_{i,j}\Theta_{i+1,j} + c^{\Theta}_{i,j}\Theta_{i-1,j} + d^{\Theta}_{i,j}\Theta_{i,j+1} + e^{\Theta}_{i,j}\Theta_{i,j-1}\}/a^{\Theta}_{i,j} \\ \hat{V}_{i,j} &= \{b^{v}_{i,j}V_{i+1,j} + c^{v}_{i,j}V_{i-1,j} + d^{v}_{i,j}V_{i,j+1} + e^{v}_{i,j}V_{i,j-1} + f^{v}_{i,j} + g^{v}_{i,j}U_{i,j}\}/a^{v}_{i,j} \end{aligned} \tag{16}$$

Numerical strategy

In order to smooth out errors due to initial guessed fields, *corrections* are defined as differences between *exact* and *not-yet-converged* variables. Residuals for momentum transport at each control volume face, continuity of mass and ϕ equations are obtained by applying the just defined *approximate* values into (6)–(11)–(15).

Taking the west face of the control volume show in Figure 1 as an example (see Equation (6)), and assuming that for a general variable ϕ a decomposition $\phi = \phi^* + \phi'$ applies, where ϕ^* is a guessed value and ϕ' a correction, one has

$$(U^* + U')_{i-1/2,j} = \hat{U}_{i-1/2,j} + \hat{d}_{i-1/2}[P_{i-1,j} - (P^* + P')_{i,j}] + \hat{e}_{i-1/2}(V^* + V')_{i,j} \tag{17}$$

For a given set of guessed or "starred" variables, Equation (6) will yield a residue, $R_{i-1/2,j}$, related to the incorrect velocity such that

$$U^*_{i-1/2,j} = \hat{U}_{i-1/2,j} + \hat{d}_{i-1/2}[P_{i-1,j} - P^*_{i,j}] + \hat{e}_{i-1/2}V^*_{i,j} - R_{i-1/2,j} \tag{18}$$

Subtracting now (18) from (17), an equation for the correction U' is obtained in the form

$$U'_{i-1/2,j} + \hat{d}_{i-1/2}P'_{i,j} - \hat{e}_{i-1/2}V'_{i,j} = R_{i-1/2,j} \tag{19}$$

Writing similar equations for all four faces, a system connecting the residuals and corrections can be written into matrix form as

$$\begin{bmatrix} 1 & 0 & 0 & 0 & \hat{d}_{i-1/2} & 0 & -\hat{e}_{i-1/2} \\ 0 & 1 & 0 & 0 & -\hat{d}_{i+1/2} & 0 & -\hat{e}_{i+1/2} \\ 0 & 0 & 1 & 0 & \hat{d}_{j-1/2} & -\hat{g}_{j-1/2} & 0 \\ 0 & 0 & 0 & 1 & -\hat{d}_{j+1/2} & -\hat{g}_{j+1/2} & 0 \\ -F_i^1 & F_i^2 & -F_j^1 & F_j^2 & 0 & 0 & 0 \\ 0 & 0 & 0 & 0 & 0 & 1 & 0 \\ 0 & 0 & 0 & 0 & 0 & 0 & 1 \end{bmatrix} \begin{bmatrix} U'_{i-1/2,j} \\ U'_{i+1/2,j} \\ W'_{i,j-1/2} \\ W'_{i,j+1/2} \\ P'_{i,j} \\ \Theta'_{i,j} \\ V'_{i,j} \end{bmatrix} = \begin{bmatrix} R_{i-1/2,j} \\ R_{i+1/2,j} \\ R_{i,j-1/2} \\ R_{i,j+1/2} \\ R_{i,j} \\ R^{\Theta}_{i,j} \\ R^{V}_{i,j} \end{bmatrix} \tag{20}$$

where the subscript identify locations in the grid, the superscript $'$ distinguishes corrections and the left hand side represents the residue vector calculated at previous iteration.

In (20) the influence of Θ on the flow field is directly accounted for by the g-terms. Similarly, the influence of V on U is implicitly considered by the e-terms. For the radial and axial directions, the g- and e-terms are of null value, respectively. As mentioned before, the reverse effect, or say the cross-flow influence on the Θ and V fields is here not treated implicitly. The solution of system (20) is then easily obtained by finding first corrections for Θ and V, calculating later the pressure P and velocity components U and W. Essentially, the method consists of finding the corrective values for U, V and P, such that the balance equations are correctly satisfied.

Computational parameters

The same relaxation parameters ($\alpha = 0.55$ for U, W, P, V and Θ) were used in all calculations. The swirling strength, S, Reynolds number, Re, and Rayleigh number, Ra, are defined as,

$$S = \frac{V}{W}\Big)_{\text{in}}, \quad \text{Re} = \frac{W_{\text{in}} 2R}{\mu}, \quad \text{Ra} = \frac{\text{Pr}\rho^2 \beta g_z \Delta \text{T} R^3}{\mu^2} \tag{21}$$

These three parameters were varied in the range $1 < S < 10^3$, $2 < \text{Re} < 10^3$ and $10^2 < \text{Ra} < 10^5$. The incoming axial velocity at inlet, W_{in}, was such that the Reynolds number, in most of the cases run, took the value in the range 2–200. This relatively small input value for W_{in} indicates that although the flow comes inside the chamber with appreciable rotation (S up to 10^3), it carries almost no momentum in the axial direction. This incoming velocity level was found to be consistent with the weak currents driven in a thermally-driven flow. With that, cases with balanced *natural* and *forced* convection mechanisms could be analyzed.

Partially segregated scheme

The algebraic equations for the velocity field were solved, in addition to the fully-coupled scheme here described, by performing outer iterations for the components Θ and V while keeping U–W–P from the previous iteration. A *line-by-line* smoothing operator, fully described elsewhere (e.g. Reference [3]), was used to relax Θ and V, being the secondary flow field (U, W) calculated by the locally-coupled method seen above. This *partially segregated*

solution was set in such a way that the same number of sweeps throughout the scalar (Θ, V) and cross-flow fields (U, W, P) was obtained. Since in the coupled scheme every sweep for U–W–P also implies in smoothing out Θ–V errors, this procedure was found to be a reasonable way to fairly compare the two methods. In all partially segregated computations, a total of four sweeps per scalar per outer iteration was performed.

The reason for recalling this second procedure a *partial* rather than a *full* segregated scheme lies in the fact that in full segregated methods all variables, including U, W and P, are solved independently and in sequence along the entire algorithm. In the case here presented for comparison, only Θ and V are excluded from the implicit treatment implied by Equation (20).

RESULTS AND DISCUSSION

Previous results and numerical accuracy

The results shown below were obtained with a previously developed numerical tool [16, 17]. The justification for using this code instead of running one of the many existing programs lies on the fact that adapting the full block-implicit arrangement shown above, involving all vector and scalar variables, would demand too much reprogramming since no pressure-correction or pressure equation is here used. Yet, to the authors' knowledge, no available source code entails exactly the same numerical formulation shown before.

Previous computations with the numerical model herein have assured the correctness and validation of the computer code developed [11–17]. Those previous results were taken after reduction of all normalized residues for mass, momentum and energy equations to the preselected value of 1×10^{-6}. Correctness of the present computer program has been checked by comparing calculations for thermally-driven flows in a square cavity with benchmark solutions reported by de Vahl Davis, 1983 [1]. Results in de Lemos [17] reproduced de Vahl Davis' calculations with less than 0.01% discrepancy for grids greater than 25×25 and $\mathrm{Ra} = 10^4$.

Similar comparisons for the exact geometry and flow conditions here analysed are more difficult to be worked on due to the scarcity of experimental data and corresponding calculations in the literature. Nevertheless, grid independence studies for the solutions herein have also been carried out (not shown here due to lack of space). For grids greater than 18×36, discrepancies in the calculations fall within 0.1%. Since the main objective of this work was to further test the proposed formulation rather than obtaining a detailed calculation of the flow, the chosen grid size was found to give accurate enough results. In summary, the results shown below should be regarded as an aid in comparing *segregated* and *coupled* solution sequences since comparisons between the performances of these two algorithms is the main focus herein.

Absolute velocities

Figure 2 shows results for the velocities at the chamber mid-planes. The figures present velocities U along the vertical z (Figure 2a, $R = 0.5$) and W along r (Figure 2b, $z = H/2 = R$), respectively. Inspecting those results one can conclude that, independently of the smoothing technique used, final converged solutions are essentially equal. The computational effort to achieve them, however, seems to be different, as it is discussed below.

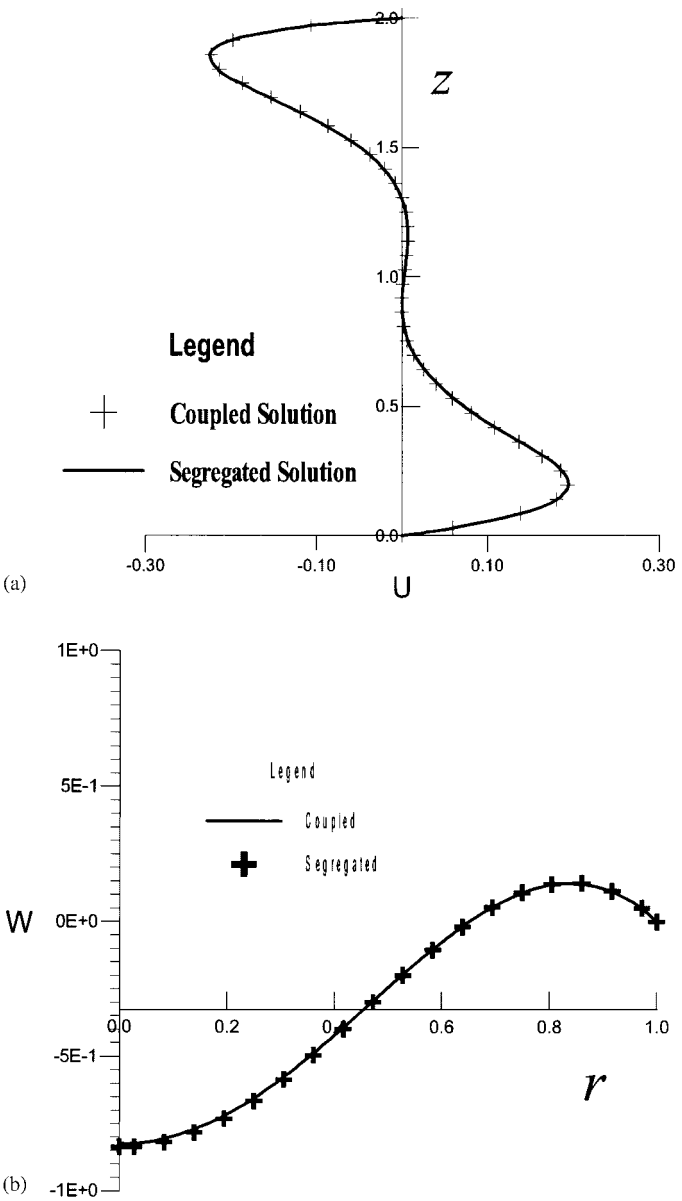

Figure 2. Radial velocity U along the z-direction at $r = 0.5$. Axial velocity along radius at $z = L/2 = R$.

Temperature field

Figure 3 shows results for the temperature field when subjected to an increase in the incoming mass flow rate (increase in Re, see Equation (21)). The figure indicates that the core of the

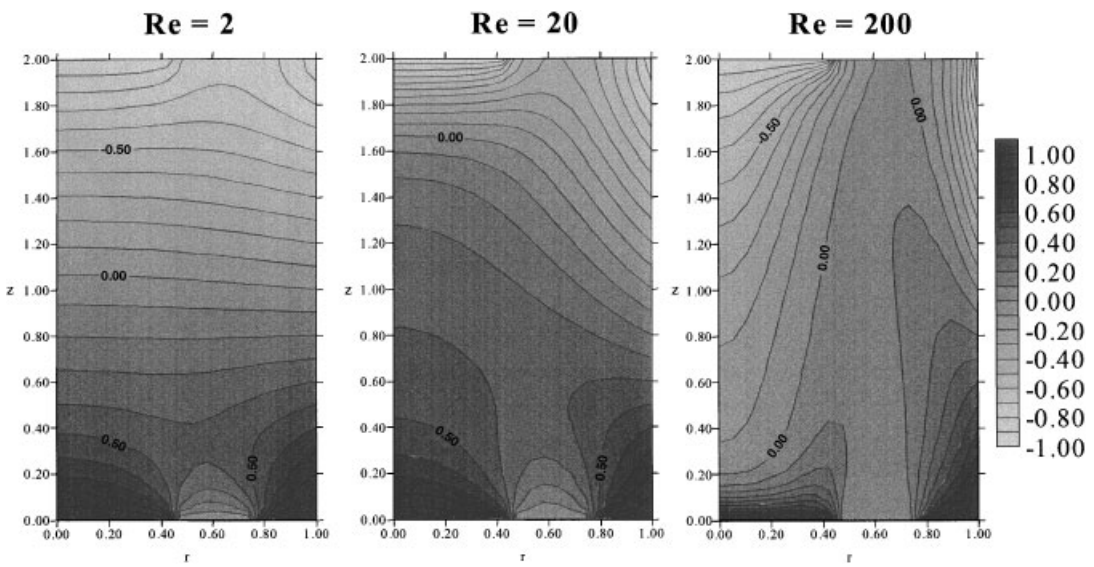

Figure 3. Effect of Re on temperature field, $S = 1$, $\mathrm{Ra} = 10^2$.

flow becomes homogenized as more fluid comes into the chamber due to higher recirculating motion in the r–z plane. Outlet temperatures are correctly increased when the higher axial mass flow rate sweeps hot fluid from bottom layers through the exit (see Figure 1 for geometry details). Increase of the central recirculating bubble is also clearly detected by the downward wash of isolines at the centerline.

Figure 4 shows calculations for the temperature field done with different values for Ra spanning from 10^2 to 10^4. Distortion of the temperature profiles also indicates strength of convective ascending currents close to the wall with corresponding downward motion at the central region. Interesting to note is the increase in temperature gradients close to the centre, at the bottom lid, due to the just mentioned downward stream. When analysing real equipment, not subjected to the imposed boundary conditions here used, steep gradients of temperature close to walls might be an indication of possible temperature raise at some particular locations. Design engineers may then use this sort of information to overcome potential material damage when performing preliminary thermal design.

Figure 5 presents the temperature pattern for different values of S. It is interesting to note the small effect on T, even though S changes by such a large factor of 10^3. Considering the assumed axi-symmetry of the flow, a strong rotation will carry fluid tangentially, essentially through zones of equal temperature. On the other hand, an increase in Re or Ra, shown in Figures 3 and 4, substantially distort the temperature by increasing the ascending cross-flow currents. One should mention that in a real fully three-dimensional flows in industrial equipment ascending currents are quite strong, playing certainly a definite role in establishing the temperature pattern inside such domains. For the simplified flow and geometry here analyzed, however, no such effect was expected.

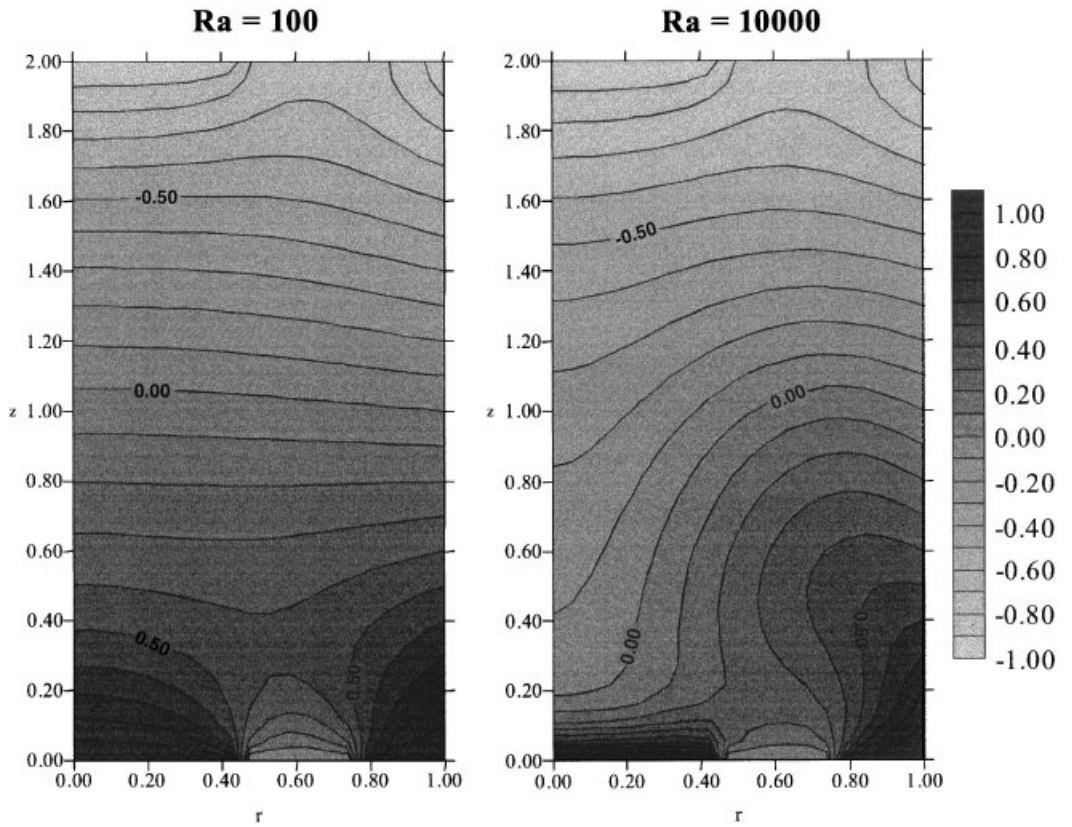

Figure 4. Effect of Ra on temperature field, $\mathrm{Re} = 2$, $S = 1$.

Residue history

Normalized residues were defined as the norm of the cell residue for mass, energy and tangential velocity equations as,

$$R_{\mathrm{abs}} = \left\{ \sum_{ij} (R_{ij})^2 / (N \cdot M) \right\}^{1/2} \tag{22}$$

where ϕ in (22) refers to the general transport variable as defined in Table I, N and M are the number of cells in the r- and z-directions, respectively. For continuity equation, R_{ij} can be seen as the difference, for every cell, between the cell *outgoing* mass flux, F_{out}, and the *incoming* mass flux, F_{in}. A *relative* mass residue can then be defined as,

$$R_{\mathrm{rel}} = \left\{ \sum_{ij} \left(\frac{F_{\mathrm{out}} - F_{\mathrm{in}}}{F_{\mathrm{out}} + F_{\mathrm{in}}} \right)^2 \Big/ (N \cdot M) \right\}^{1/2} \tag{23}$$

A discussion on the advantages in simultaneously monitoring R_{rel} in addition to R_{abs} is presented in de Lemos [11, 12, 17] and it is based on the small range of the former $(0, +1)$. Equation (23) can be seen as normalization for the residue values for cases ranging from a

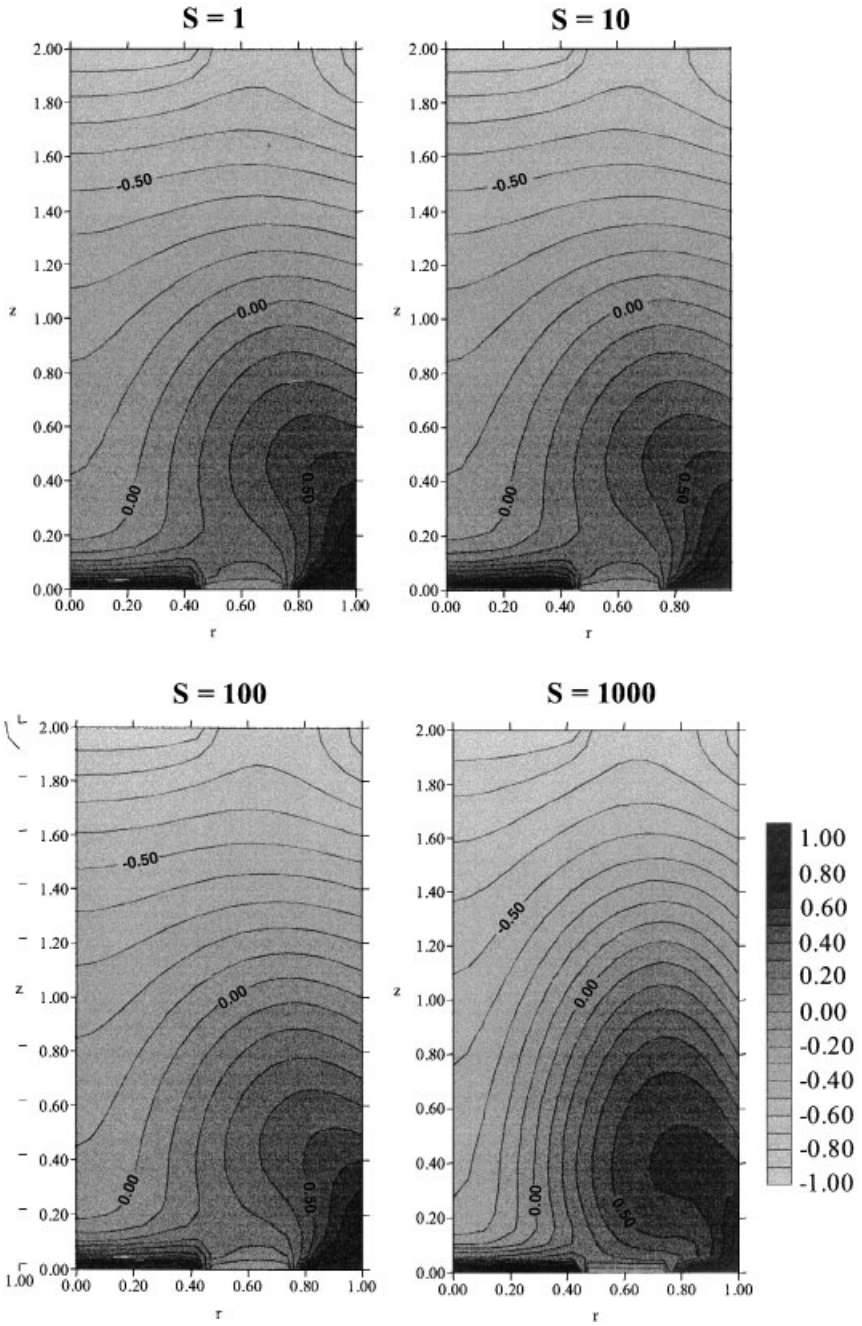

Figure 5. Effect of swirling strength on temperature, $\mathrm{Ra} = 10^4$, $\mathrm{Re} = 2$.

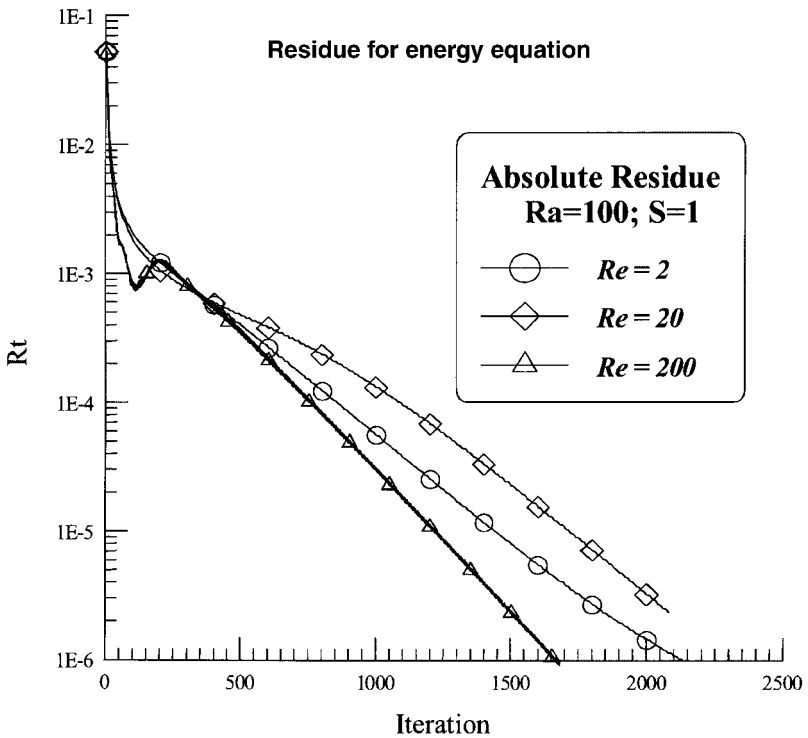

Figure 6. Influence of Re on convergence rate of T-equation.

totally "incorrect" field ($F_{out} = -F_{in}$, $R_{rel} = 1$) to a perfectly "converged" solution ($F_{out} = F_{in}$, $R_{rel} = 0$).

The three parameters here investigated, namely Re, Ra and S, were analysed in terms of their influence on the overall convergence rates. Results are shown in Figures 6, 7 and 8, respectively. The iteration counter refers to the total number of sweeps over the domain, that is, the product of the outer counter times the number of inner sweeps. Here, a quick word on the numbers of iterations to convergence seems timely. Other schemes presented in the literature may indicate residue history as a function of outer iteration counters only. Some, use the so-called pseudo-transient approach and plot time steps instead. Each outer iteration, in turn, may consider a great number of internal sweeps, usually controlled by a specified residue reduction rate. Here, in this work, a fixed number of internal sweeps was considered. The relatively large number of necessary iterations seen in the figures below could be associated with the use of a single grid, the tightness of the relaxation parameters and the strong coupling among all variables involved. Ultimately, all of these factors together tend to delay convergence.

It is interesting to note that the better convergence performance for the higher Reynolds number (see Figure 6), possibly reflecting the fact that, as Re increases, the flow becomes more *forced-convection* dominated decreasing the *UW–T* coupling in relation to the *UW–P* connection. This, in turn, facilitates the solution of the energy equation once the velocity field is calculated. This idea is supported when Figure 7 is inspected, showing worse convergence

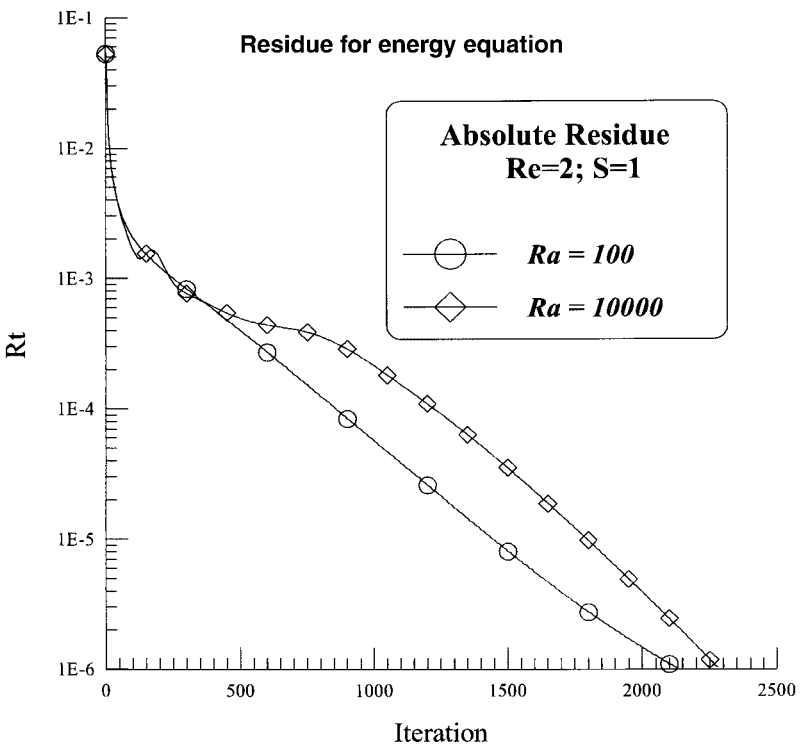

Figure 7. Effect of Ra on R_T.

rates for a higher Ra. There, the higher degree of coupling between temperature and cross-flow fields makes computation more demanding, reflecting the increase in physical coupling among the flow variables and temperature.

On the other hand, when S is varied, Figure 8 shows a weak dependency of R_T on the swirling strength. According to Figure 5, no substantial change on temperature patterns was detected when inlet rotation increases (except for $S = 10^3$). For such small inlet mass flow rates ($\mathrm{Re} = 2$), viscous shear driven by the incoming swirling motion enhances the cross-flow field which, in turn, distorts isothermal lines. Such an indirect or second-order relationship between V and T is apparently also reflected on the residue histories shown in Figure 8.

Mass residues, calculated by Equations (22) and (23), are presented in Figure 9 indicating that, after an initial period when low frequency errors are damped, a better convergence rate is obtained with the coupled method in either form of residue.

Residue histories for the temperature and tangential velocity fields are presented in Figures 10 and 11, respectively. For the *coupled* strategy, a quicker reduction for the residue is obtained, since in each sweep, for every cell, information on all variables propagates at the same "time rate". Also, the figures show that the *segregated* method, for the case here analysed, use as many as 20–30% more iterations to bring R_V down to the same level as the coupled scheme and nearly two times as many outer sweeps to reduce to the same value of R_T. Although the computational effort per field sweep in both schemes are not necessarily equal, due to the fact that the number of floating point operations per iteration in the two

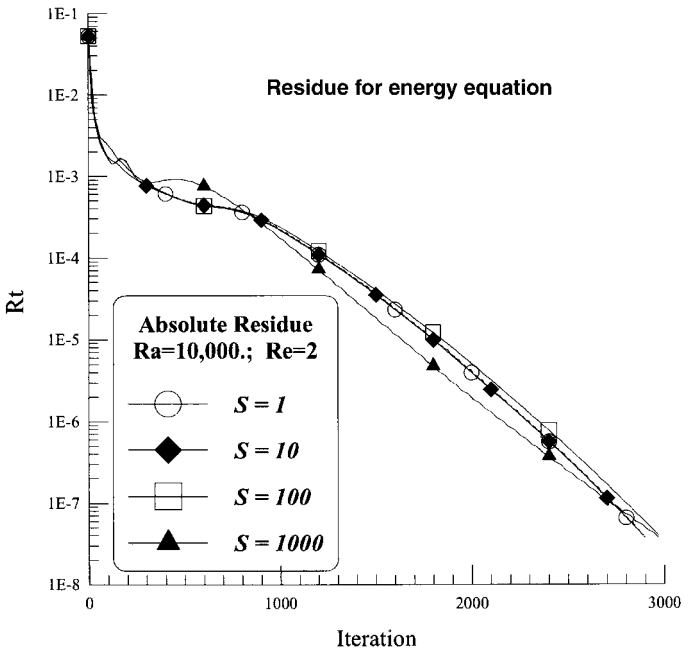

Figure 8. Effect of swirling strength S on R_T.

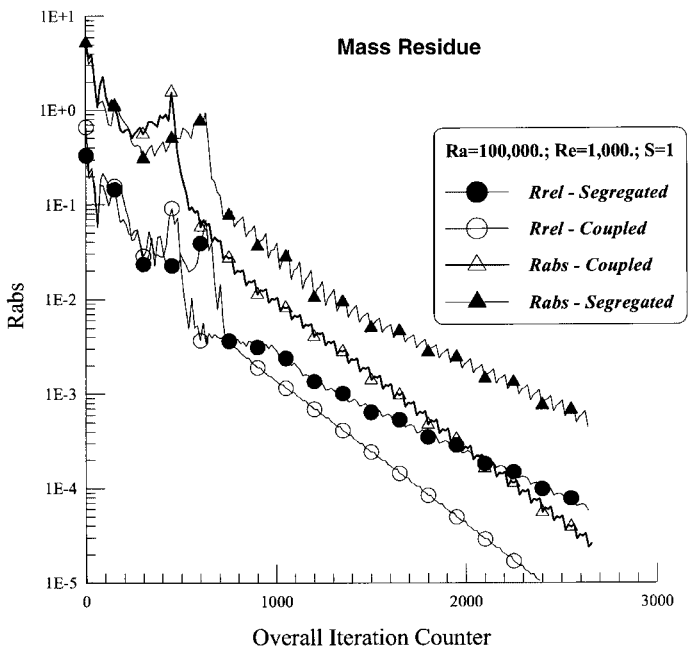

Figure 9. Mass residue history for segregated and coupled approaches.

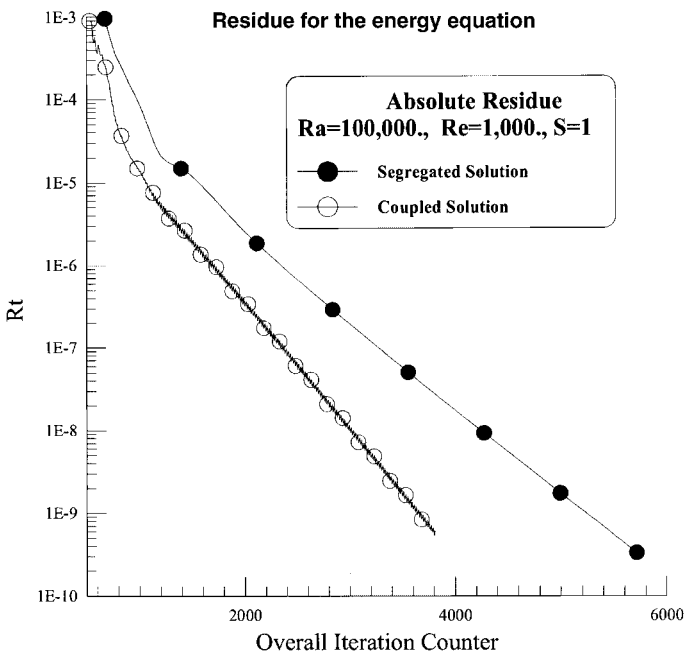

Figure 10. Influence of solution scheme on residue history of energy equation.

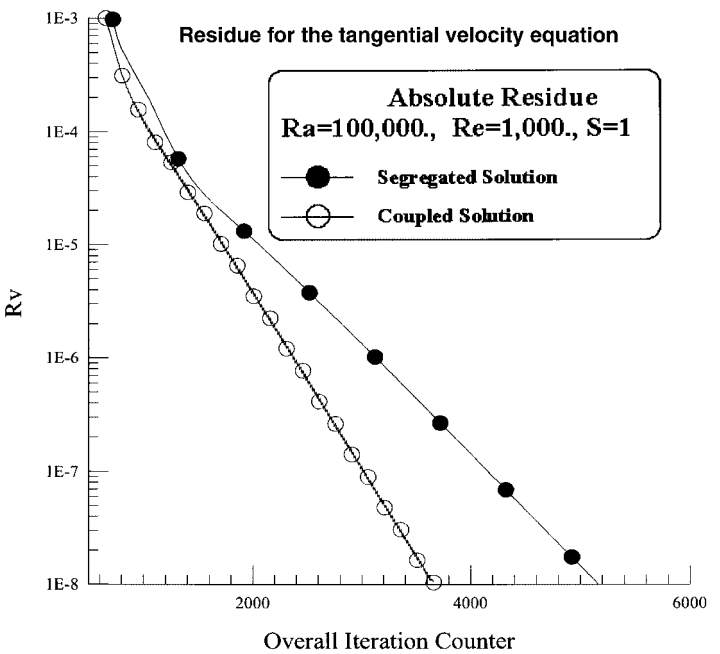

Figure 11. Influence of solution scheme on convergence of *V*-equation.

algorithms are not the same, a primary consequence of the foregoing is that a relatively longer computing time is expected when the decoupled solution is used with the same convergence criteria applied to the scalar equations.

Finally, Figures 10 and 11 seem to indicate also that the cross-flow field can quickly adjust itself to changes in the scalar profiles, and that, in the segregated case, those changes are too slowly transferred back to Θ–V. The coupled solution, however, quickly transmits back to Θ *and* V-equations changes in the cross-flow pattern, more realistic simulating the strong interaction among the variables involved.

CONCLUDING REMARKS

This paper detailed a fully-coupled technique for numerical prediction of ascending heated swirling flows in a cylindrical chamber. An extension of the numerical method in Vanka, 1986 [9, 10] towards a fully implicit solution of the energy, tangential and cross-flow equations was reported. Outline of the numerical method showed the necessary steps for setting up the residuals and the methodology used to calculate the corrections for all dependent variables. Comparison of partially-segregated and fully-coupled treatments for the energy and tangential velocity shows a lower computer effort when the latter method was used. The approach herein is promising regarding numerical stability of the entire equation set since inherent coupling among the variables is implicitly handled. Further, it is also expected that more advanced multi-processor computer architectures can benefit from the point wise error smoothing operator here described. Ultimately, different processors can simultaneously solve block of control-volumes, possibly reducing the overall computational effort when comparisons are made with the sequential calculation procedure used by segregated algorithms.

NOMENCLATURE

a–g	coefficients in the finite-difference equations
β	thermal expansion coefficient
$F's$	coefficients for continuity equation
g_z	z-component of gravity vector
H	chamber height
M	number of cells in the axial direction
N	number of cells in the radial direction
P	pressure
Pr	Prandtl number
R	model combustor radius
Ra	Rayleigh number
R_{abs}	absolute residue for mass continuity equation
R_{rel}	relative residue for mass continuity equation
R_T	residue for the energy equation
R_V	residue for the tangential velocity equation
Re	Reynolds number
S	swirl parameter
S^ϕ	source term

T temperature, $T_1 = \max.$ Temp., $T_0 = \min.$ Temp.
U radial velocity component
W axial velocity component
W_{in} inlet axial velocity
V tangential velocity component
Γ^{ϕ} transport coefficient for variable $\phi = U, W, V, \Theta$
μ fluid dynamic viscosity
ρ fluid density
ϕ general dependent variable, $\phi = U, W, V, \Theta$
Θ non-dimensional temperature: $\Theta = (T - T_0)/(T_1 - T_0)$

ACKNOWLEDGEMENTS

The author is grateful to CNPq, Brazil, for their financial support during the preparation of this work.

REFERENCES

1. de Vahl Davis G. Natural convection of air in a square cavity: a bench mark numerical solution. *International Journal for Numerical Methods in Fluids* 1983; **3**:249–264.
2. Hortmann M, Periç M, Scheider G. Finite volume multigrid predictions of laminar natural convection: benchmark solutions. *International Journal for Numerical Methods in Fluids* 1990; **11**:189–207.
3. Patankar SV. *Numerical Heat Transfer and Fluid Flow*. McGraw-Hill: New York, 1980.
4. Galpin PF, Raithby GD. Numerical solution of problems in incompressible flow: temperature of the temperature velocity coupling. *Numerical Heat Transfer* 1986; **9**(1):105–129.
5. Tang L, Joshi YK. Application of block implicit multigrid approach to three-dimensional heat transfer problems involving discrete heating. *Numerical Heat Transfer—Part A* 1999; 35:717–734.
6. Hogg S, Leschiziner MA. Second-moment-closure calculation of strongly swirling confined flow wit large density gradients. *International Journal of Heat and Fluid Flow* 1989; **10**(1):16–27.
7. Hogg S, Leschiziner MA. Computation of highly swirling confined flow with as Reynolds stress turbulence model. *AIAA Journal* 1989; **27**(1):57–63.
8. Nikjook M, Mongia HC. A second-order modeling study of confined swirling flows. *International Journal of Heat and Fluid Flow* 1991; **12**(1):12–19.
9. Vanka SP. A calculation procedure for three-dimensional steady recirculating flows using multigrid methods. *Computer Methods in Applied Mechanics and Engineering* 1986; **55**:321–338.
10. Vanka SP. Block-implicit multigrid solution of Navier–Stokes equations in primitive variables. *Journal of Computational Physics* 1986; **65**:138–158.
11. de Lemos MJS. Computation of laminar axi-symmetric recirculating flows using primitive variables and a block-implicit scheme. *Proceedings of the ENCIT90—3rd Braz. Therm. Sci. Meeting*, vol. 1, Itapema, SC, Brazil, 10–12 December 1990; 375–380.
12. de Lemos MJS. Simulation of swirling flow in a model combustor using a locally-coupled numerical method. *Proceedings of the Winter Annual Meeting of the ASME 1992*, vol. HTD-226, Anaheim, CA, USA, 8–13 November 1992; 79–84.
13. de Lemos MJS. Computation of buoyancy-driven flows using a block-implicit numerical scheme. *Proceedings of the 28th Nat. Heat Transfer Conference* 1992, vol. HTD-194, San Diego, CA, USA, 9–12 August 1992; 83–89.
14. de Lemos MJS. Locally-coupled numerical solution of thermally-driven cavity flows. *Proceedings of COBEM97—14th Braz. Congr. Mech. Eng.*, Bauru, SP, Brazil, 8–12 December 1997.
15. de Lemos MJS. Cell-implicit numerical computation of flow field and heat transfer in inclined cavities. *Proceedings of COBEM97—14th Braz. Congr. Mech. Eng.*, (on CD-ROM), Bauru, SP, Brazil, 8–12 December 1997.
16. de Lemos MJS. A block-implicit method for numerical simulation of swirling flows in a model combustor. *International Communications of Heat and Mass Transfer* 2003; **30**:369–378.
17. de Lemos MJS. Flow and heat transfer in rectangular enclosures using a new block implicit numerical method. *Numerical Heat Transfer—Part B* 2000; **37**(4):489–508.
18. Rabi JA, de Lemos MJS. Optimization of convergence acceleration in multigrid numerical solutions of conductive-convective problems. *Applied Mathematics and Computation* 2001; **124**(2):215–226.

